Electronic Supplementary Information

Non-oxidative dehydrogenation of propane, n-butane, and isobutane over bulk ZrO_2-based catalysts: Effect of dopant on active site and pathways of product formation

Tatiana P. Otroshchenko, Vita A. Kondratenko, Uwe Rodemerck, David Linke, Evgenii V. Kondratenko*

Leibniz-Institut für Katalyse e. V. an der Universität Rostock, Albert-Einstein-Str. 29 A D-18059 Rostock, Germany

* To whom correspondence should be addressed. E-mail: Evgenii.kondratenko@catalysis.de

Mears Criterion for External Diffusion Limitations

External diffusion limitations are negligible if

$$\frac{r_{obs} \cdot \rho_{catalyst} \cdot R \cdot n}{k_c \cdot C} < 0.15$$

r_{obs} – measured reaction rate, kmol/(kg_{cat}·s)

$\rho_{catalyst}$ – catalyst density, kg/m^3

R – catalyst pellet radius, m

n – reaction order

k_c – mass transfer coefficient, m/s

C – bulk concentration of reactant, kmol/m^3

For propane dehydrogenation at 600°C over the most active catalyst $Y_9Zr_{91}O_x$:

$\frac{r_{obs} \cdot \rho_{catalyst} \cdot R \cdot n}{k_g \cdot C}$ = [$1.44 \cdot 10^{-5}$ kmol/(kg_{cat}·s)]·[$9.47 \cdot 10^{2}$ kg/m^3]·[$3.5 \cdot 10^{-4}$ m]·1/([$2.14 \cdot 10^{-1}$ m/s]·[$5.51 \cdot 10^{-3}$ kmol/m^3]) = **$4.04 \cdot 10^{-3}$ < 0.15**

For n-butane dehydrogenation at 600°C over the most active catalyst $Y_9Zr_{91}O_x$:

$\frac{r_{obs} \cdot \rho_{catalyst} \cdot R \cdot n}{k_g \cdot C}$ = [$2.09 \cdot 10^{-5}$ kmol/(kg_{cat}·s)]·[$9.47 \cdot 10^{2}$ kg/m^3]·[$3.5 \cdot 10^{-4}$ m]·1/([$3.03 \cdot 10^{-1}$ m/s]·[$5.51 \cdot 10^{-3}$ kmol/m^3]) = **$4.14 \cdot 10^{-3}$ < 0.15**

For iso-butane dehydrogenation at 600°C over the most active catalyst $Y_9Zr_{91}O_x$:

$\frac{r_{obs} \cdot \rho_{catalyst} \cdot R \cdot n}{k_g \cdot C}$ = [$3.70 \cdot 10^{-5}$ kmol/(kg_{cat}·s)]·[$9.47 \cdot 10^{2}$ kg/m^3]·[$3.5 \cdot 10^{-4}$ m]·1/([$3.03 \cdot 10^{-1}$ m/s]·[$5.51 \cdot 10^{-3}$ kmol/m^3]) = **$7.35 \cdot 10^{-3}$ < 0.15**

Weisz-Prater criterion for Internal Diffusion Limitations

To estimate the influence of internal diffusion on the reaction rates, we used Weisz-Prater criterion.

$$\Psi = \frac{n+1}{2} \cdot \frac{r \cdot \rho_{catalyst} \cdot R^2}{D \cdot C} \quad \text{(S1)}$$

If $\Psi < 1$, internal diffusion limitations are negligible

n – reaction order

r_{obs} – measured reaction rate, kmol/(kg_{cat}·s)

$\rho_{catalyst}$ – catalyst density, kg/m^3

R – catalyst pellet radius, m

D – diffusion coefficient, m^2/s

C – bulk concentration of reactant, kmol/m^3

For propane dehydrogenation at 600°C over the most active catalyst $Y_9Zr_{91}O_x$:

Ψ = [(1 + 1)/2] [$1.44\cdot 10^{-5}$ kmol/(kg_{cat}·s)]·[$9.47\cdot 10^{2}$ kg/m^3]·[$(3.5\cdot 10^{-4})^2$ m^2]/([$1\cdot 10^{-4}$ m^2/s]·[$5.51\cdot 10^{-3}$ kmol/m^3]) = **$3.03\cdot 10^{-3}$ < 1**

For n-butane dehydrogenation at 600°C over the most active catalyst $Y_9Zr_{91}O_x$:

Ψ = [(1 + 1)/2] [$2.09\cdot 10^{-5}$ kmol/(kg_{cat}·s)]·[$9.47\cdot 10^{2}$ kg/m^3]·[$(3.5\cdot 10^{-4})^2$ m^2]/([$1\cdot 10^{-4}$ m^2/s]·[$5.51\cdot 10^{-3}$ kmol/m^3]) = **$4.39\cdot 10^{-3}$ < 1**

For iso-butane dehydrogenation at 600°C over the most active catalyst $Y_9Zr_{91}O_x$:

Ψ = [(1 + 1)/2] [$3.70\cdot 10^{-5}$ kmol/(kg_{cat}·s)]·[$9.47\cdot 10^{2}$ kg/m^3]·[$(3.5\cdot 10^{-4})^2$ m^2]/([$1\cdot 10^{-4}$ m^2/s]·[$5.51\cdot 10^{-3}$ kmol/m^3]) = **$7.79\cdot 10^{-3}$ < 1**

Mears Criterion for External Heat Transfer Limitations

External heat transfer limitations are negligible if

$$\frac{r_{obs}\cdot\rho_{catalyst}\cdot R\cdot E_a\cdot\Delta H}{k_g\cdot R_g\cdot T^2} < 0.15$$

r_{obs} – measured reaction rate, kmol/(kg_{cat}·s)

$\rho_{catalyst}$ – catalyst density, kg/m^3

R – catalyst pellet radius, m

E_a – activation energy, kJ/kmol

ΔH – reaction heat, kJ/mol

k_g – heat transport coefficient, kJ/(m^2·s·K)

R_g – gas constant, kJ/(mol·K)

T – reaction temperature, K

For propane dehydrogenation at 600°C over the most active catalyst $Y_9Zr_{91}O_x$:

$\frac{r_{obs} \cdot \rho_{catalyst} \cdot R \cdot E_a \cdot \Delta H}{k_g \cdot R_g \cdot T^2}$ = [1.44· 10^{-5} kmol/(kg_{cat}· s)]· [9.47· 10^2 kg/m^3]· [3.5· 10^{-4} m]· [1.20· 10^5 kJ/kmol]· [1.29· 10^2 kJ/mol]/([1.46 kJ/(m^2· s· K)]· [8.31· 10^3 kJ/(mol· K)]· [(8.73· 10^2)^2 K^2]) = **8.02· 10^{-3} < 0.15**

For n-butane dehydrogenation at 600°C over the most active catalyst $Y_9Zr_{91}O_x$:

$\frac{r_{obs} \cdot \rho_{catalyst} \cdot R \cdot E_a \cdot \Delta H}{k_g \cdot R_g \cdot T^2}$ = [2.09· 10^{-5} kmol/(kg_{cat}· s)]· [9.47· 10^2 kg/m^3]· [3.5· 10^{-4} m]· [1.05· 10^5 kJ/kmol]· [1.30· 10^2 kJ/mol]/([2.06 kJ/(m^2· s· K)]· [8.31· 10^3 kJ/(mol· K)]· [(8.73· 10^2)^2 K^2]) = **7.24· 10^{-3} < 0.15**

For isobutane dehydrogenation at 600°C over the most active catalyst $Y_9Zr_{91}O_x$:

$\frac{r_{obs} \cdot \rho_{catalyst} \cdot R \cdot E_a \cdot \Delta H}{k_g \cdot R_g \cdot T^2}$ = [3.70· 10^{-5} kmol/(kg_{cat}· s)]· [9.47· 10^2 kg/m^3]· [3.5· 10^{-4} m]· [1.28· 10^5 kJ/kmol]· [1.23· 10^2 kJ/mol]/([2.06 kJ/(m^2· s· K)]· [8.31· 10^3 kJ/(mol· K)]· [(8.73· 10^2)^2 K^2]) = **1.48· 10^{-2} < 0.15**

Figures

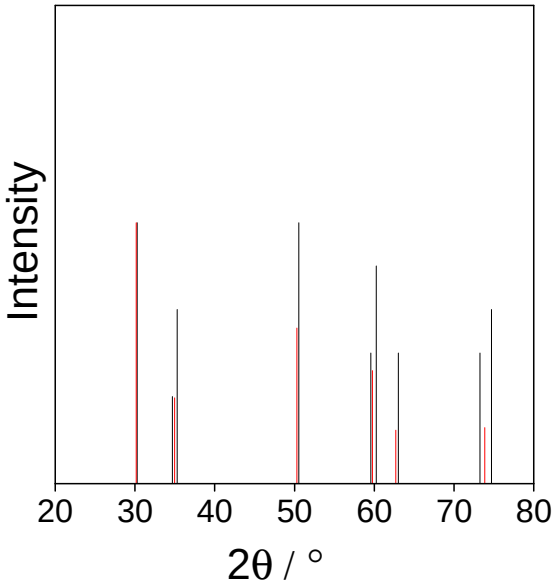

Figure S 1. Data base XRD patterns of ZrO_2: black bars are related to t-ZrO_2 (PDF-No. 00-014-0534) and red bars – to c-ZrO_2 (PDF-No. 01-078-5752).

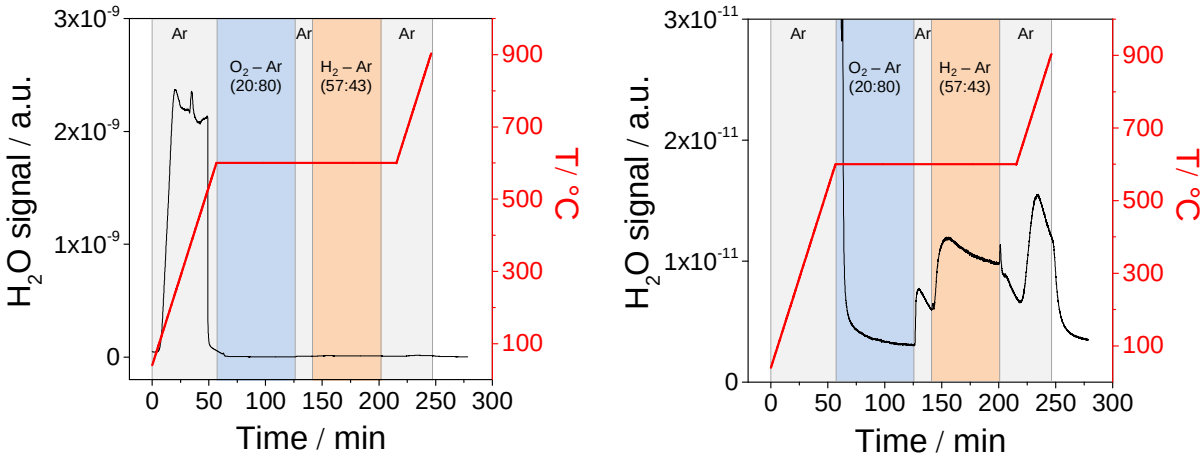

Figure S 2. Water released upon thermal treatment of $La_8Zr_{92}O_x$ in different feeds (Ar, 20 vol.% O_2 – 80 vol.% Ar, or 57 vol.% H_2 – 43 vol.% Ar). The axis Y in the right figure is zoomed for clear illustration of H_2O formation upon catalyst reduction and heating to 900°C.

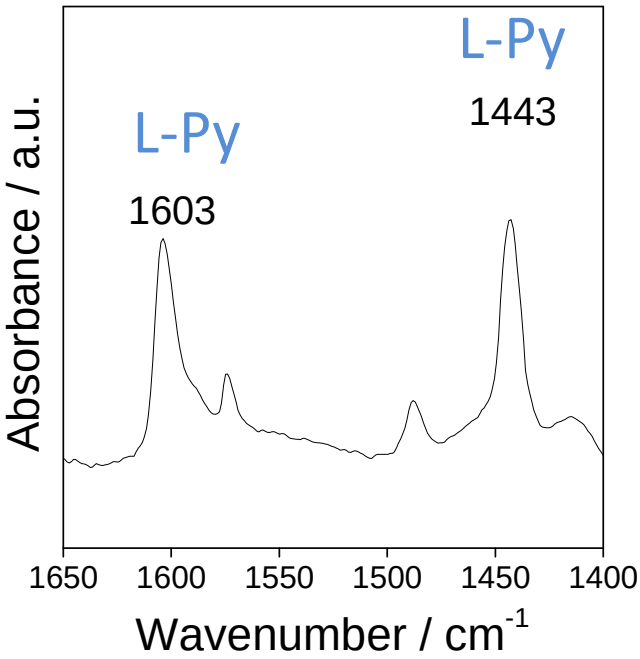

Figure S 3. The infrared spectrum of pyridine adsorbed on reduced $Y_9Zr_{91}O_x$. The bands at 1603 and 1443 cm^{-1} are characteristic for Lewis acidic sites.

For discriminating between Brønsted and Lewis acidic sites, we performed IR measurements of adsorbed pyridine on a Tensor 27 spectrometer (Bruker). Prior to the measurement, $Y_9Zr_{91}O_x$ was heated up in N_2 flow to 600°C, calcined in air flow at this temperature for 1 hour, flushed with N_2 flow for 15 min and reduced in H_2 flow (57 vol.% H_2 in N_2) for 1 hour. Hereafter, the catalyst was cooled down in N_2 flow to room temperature. So treated sample were pressed into self-supporting wafers with a diameter of 20 mm. Prior to pyridine adsorption, it was again treated in the IR cell according to the following protocol: heating in air to 450°C for 1 hour, flushing with N_2 for 15 min, treating in H_2 flow (57 vol.% H_2 in N_2) for 1 hour. Hereafter, the catalyst was cooled down in N_2 flow to room temperature. Pyridine was adsorbed at 25°C until saturation. Then the reaction cell was evacuated for removing physisorbed pyridine. After heating the sample in vacuum to 100°C, the IR spectrum of adsorbed pyridine was recorded.

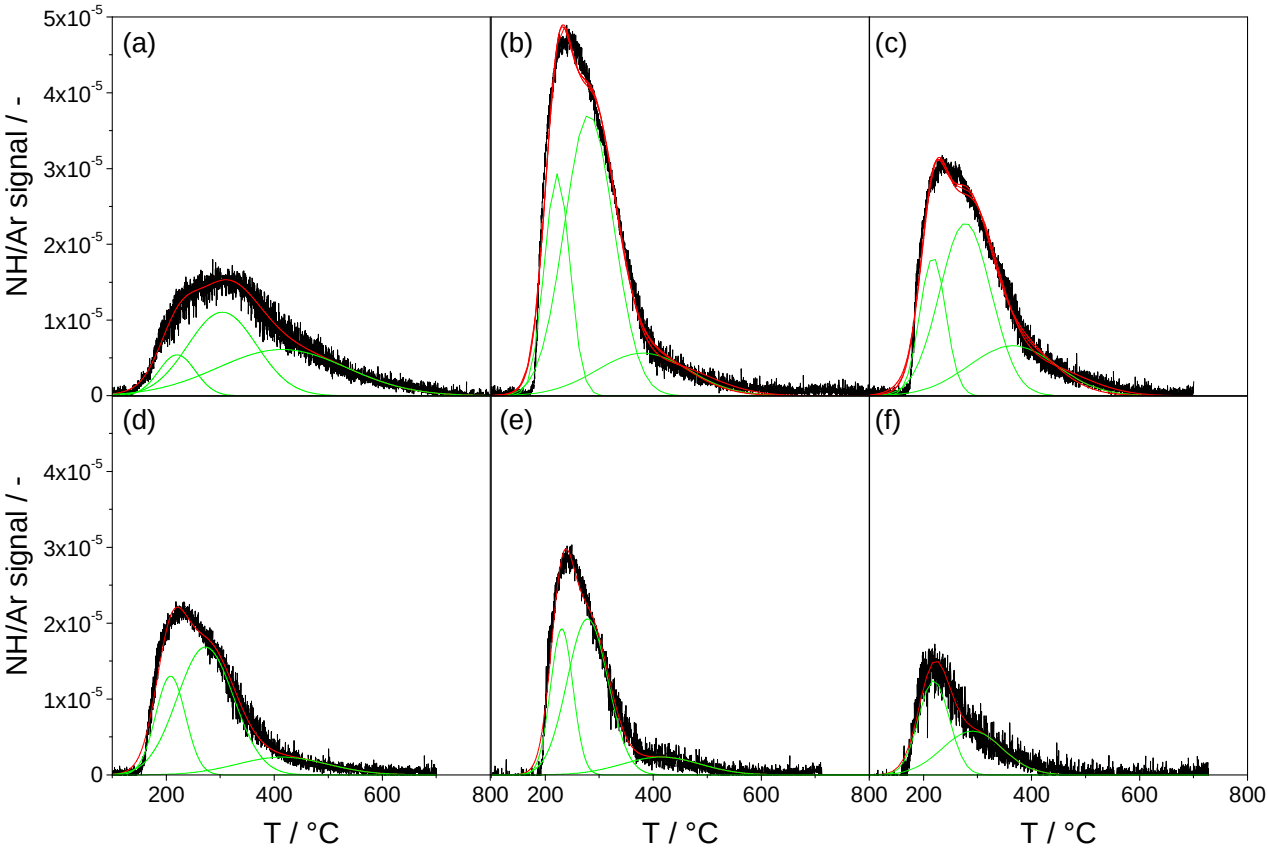

Figure S 4. Fitting of NH_3-TPD peaks obtained for reduced (a) ZrO_2, (b) $La_8Zr_{92}O_x$ (c) $Y_9Zr_{91}O_x$ (d) $Sm_{10}Zr_{90}O_x$, (e) $Ca_{10}Zr_{90}O_x$, (f) $Mg_{10}Zr_{90}O_x$.

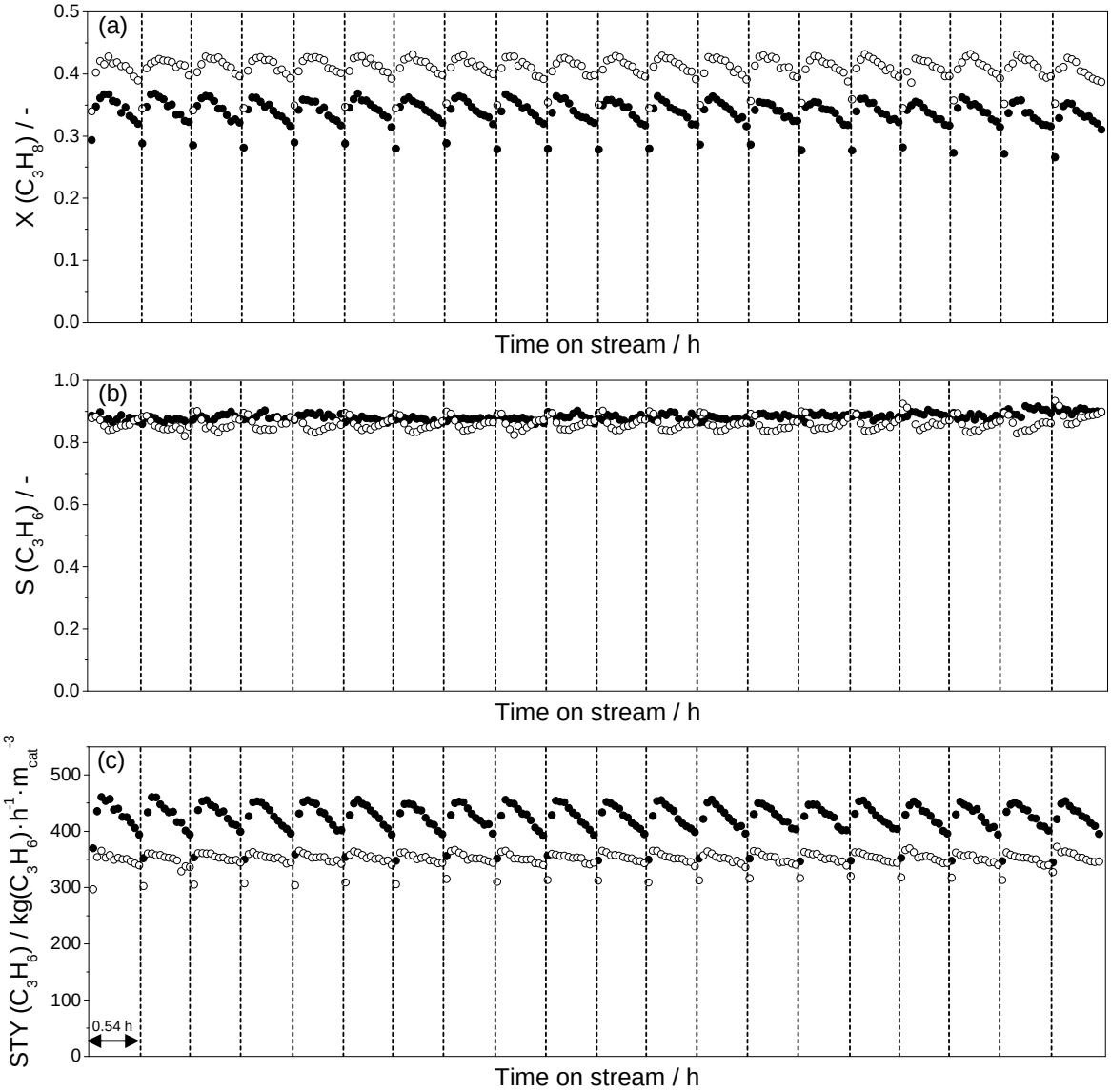

Figure S 5. Temporal change of (a) propane conversion, (b) propene selectivity and (c) propene space time yield for each DH stage in a series of 20 propane DH/regeneration cycles at 550°C over ● $Y_9Zr_{91}O_x$ and ○ K-CrO_x/Al_2O_3 catalysts.

Long-term stability of $Y_9Zr_{91}O_x$ and ○ K-CrO_x/Al_2O_3 was checked in a series of 20 propane DH/regeneration cycles at 550°C using a feed with 40 vol.% C_3H_8 in N_2 at WHSV of 1.6 h^{-1} with respect to propane. The catalyst amount was fixed to 300 mg. The regeneration was performed in an air flow. The DH and regeneration cycles lasted for about 35 and 30 min respectively and were always separated by a phase of flushing with N_2 lasting for 15 min.

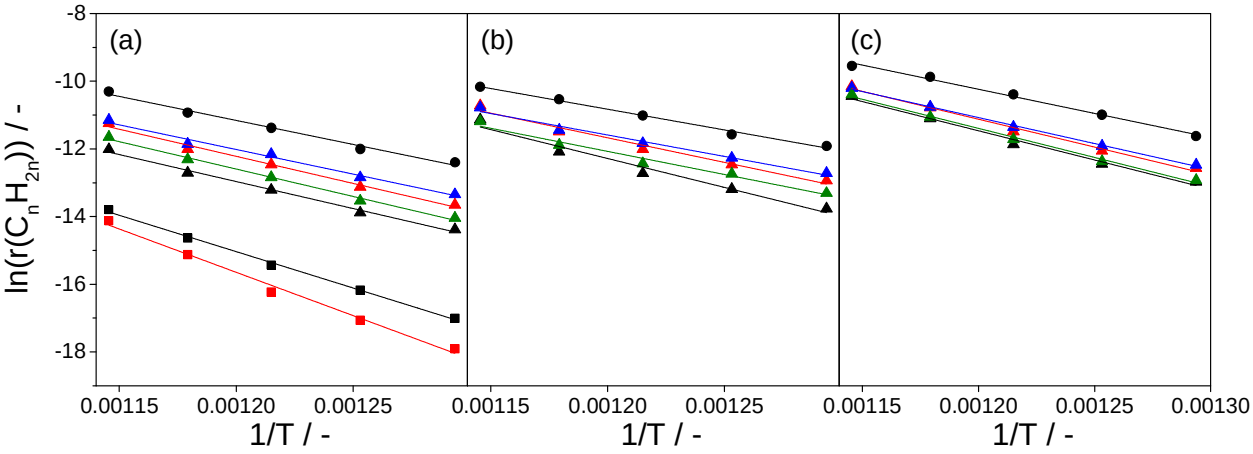

Figure S 6. Arrhenius plots of (a) propene, (b) n-butenes, and (c) isobutene formation in DH of propane, n-butane, and isobutane, respectively, over reduced ▲ ZrO_2, ▲ $La_8Zr_{92}O_x$, ▲ $Y_9Zr_{91}O_x$, ▲ $Sm_{10}Zr_{90}O_x$, ■ $Ca_{10}Zr_{90}O_x$, ■ $Mg_{10}Zr_{90}O_x$, and ● K-CrO_x/Al_2O_3 catalysts.

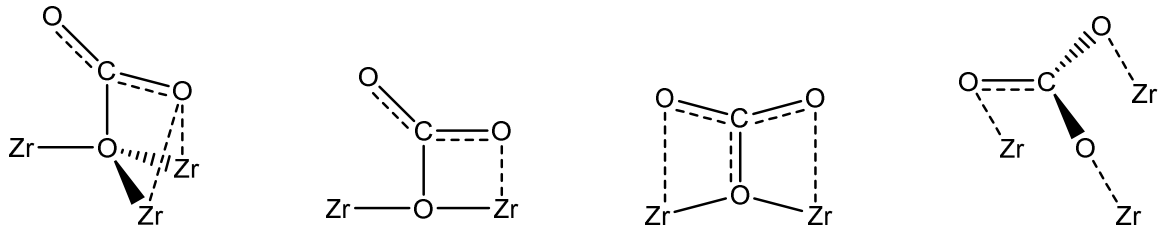

Figure S 7. Different kinds of surface carbonates formed as a result of CO_2 adsorption on ZrO_2 surface.

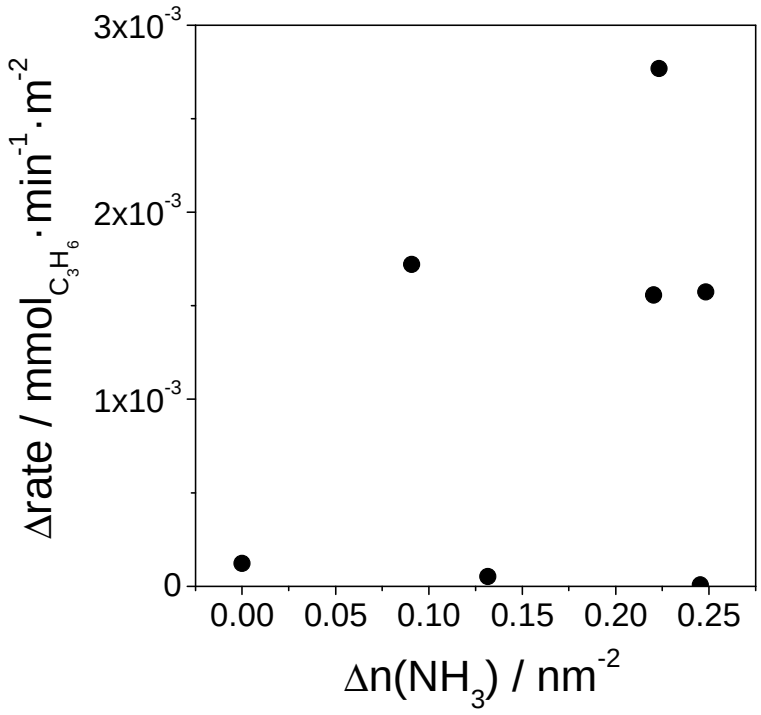

Figure S 8. The difference (Δrate) between the rate of propene formation over reduced and oxidized samples (equation 1) versus the difference ($\Delta n(NH_3)$) between the number of acidic sites in oxidized and reduced catalysts (equation 2).

$$\Delta rate = rate(reduced\ catalysts) - rate(oxidized\ catalysts) \quad (1)$$

$$\Delta n(NH_3) = n(NH_3)(reduced\ samples) - n(NH_3)\ (oxidized\ catalysts) \quad (2)$$

Table S 1. Maxima of NH_3-TPD desorption peaks in °C and corresponding amount of desorbed NH_3 related to nm^2 (numbers in brackets) for reduced samples.

Sample	1st peak	2nd peak	3rd peak
ZrO_2	220 (0.15)	304 (0.57)	415 (0.60)
$La_8Zr_{92}O_x$	223 (0.25)	283 (0.67)	415 (0.14)
$Y_9Zr_{91}O_x$	219 (0.16)	281 (0.57)	415 (0.14)
$Sm_{10}Zr_{90}O_x$	208 (0.199)	273 (0.46)	415 (0.10)
$Ca_{10}Zr_{90}O_x$	231 (0.13)	279 (0.25)	415 (0.06)
$Mg_{10}Zr_{90}O_x$	219 (0.35)	291 (0.32)	-
$Li_{10}Zr_{90}O_x$	-	-	-

Table S 2. Product distribution for propane dehydrogenation obtained for each catalyst at C_3H_8 conversion between 17 and 22%.

Catalyst	X(C_3H_8)	S(C_3H_6)	S(CH_4)	S(C_2H_4)	S(CO)	S(coke)
ZrO_2	0.17	0.795	0.007	0.003	0.003	0.192
$La_8Zr_{92}O_x$	0.21	0.974	0.005	0.001	0.003	0.017
$Y_9Zr_{91}O_x$	0.22	0.972	0.007	0.002	0.002	0.017
$Sm_{10}Zr_{90}O_x$	0.22	0.917	0.012	0.003	0.007	0.061
K-CrO_x/Al_2O_3	0.21	0.97	0.006	0.005	0.001	0.018

Table S 3. Product distribution for isobutane dehydrogenation obtained for each catalyst at iso-C_4H_{10} conversion between 17 and 23%.

Catalyst	X(iso-C_4H_{10})	S(iso-C_4H_8)	S(1-C_4H_8)	S(cis-2-C_4H_8)	S(trans-2-C_4H_8)	S(CH_4)	S(C_3H_6)	S(coke)
ZrO_2	0.21	0.75	0.006	0.005	0.007	0.01	0.011	0.211
$La_8Zr_{92}O_x$	0.23	0.943	0	0	0	0.003	0.005	0.049
$Y_9Zr_{91}O_x$	0.18	0.938	0	0	0	0.004	0.005	0.053
$Sm_{10}Zr_{90}O_x$	0.17	0.931	0	0	0	0.005	0.007	0.057
K-CrO_x/Al_2O_3	0.21	0.93	0	0	0	0.002	0.006	0.062

Table S 4. Product distribution for n-butane dehydrogenation obtained for each catalyst at n-C_4H_{10} conversion between 15 and 20%.

Catalyst	X(n-C_4H_{10})	S(1-C_4H_8)	S(cis-2-C_4H_8)	S(trans-2-C_4H_8)	S(1,2-C_4H_6)	S(CH_4)	S(C_2H_6)	S(C_3H_8)	S(C_3H_6)	S(CO)	S(coke)
ZrO_2	0.18	0.267	0.247	0.31	0.092	0.005	0	0.001	0.004	0.004	0.07
$La_8Zr_{92}O_x$	0.20	0.286	0.265	0.333	0.107	0	0	0.001	0	0.001	0.007
$Y_9Zr_{91}O_x$	0.17	0.282	0.262	0.327	0.1	0	0	0.002	0	0.001	0.026
$Sm_{10}Zr_{90}O_x$	0.17	0.28	0.259	0.323	0.107	0.003	0.001	0.003	0	0.002	0.022
K-CrO_x/Al_2O_3	0.15	0.275	0.262	0.31	0.145	0.001	0.003	0.003	0	0.001	0